Quantifying the factors limiting performance and rates in microbial fuel cells using the electrode potential slope analysis combined with electrical impedance spectroscopy

Ruggero Rossi[1], Derek M. Hall[2], Xu Wang[1,3], John M. Regan[1],
Bruce E. Logan[1]*

[1]Department of Civil and Environmental Engineering, The Pennsylvania State University, 231Q Sackett Building, University Park, PA 16802, USA
[2]EMS Energy Institute, College of Earth and Mineral Sciences, The Pennsylvania State University, 206 Academic Projects, University Park, PA 16802, USA
[3]School of Resource and Environmental Sciences, Hubei International Scientific and Technological Cooperation Base of Sustainable Resource and Energy, Wuhan University, 129 Luoyu Road, Wuhan 430079, PR China

*Corresponding author: e-mail: blogan@psu.edu; phone: +1-814-863-7908; fax: +1-814-863-7304

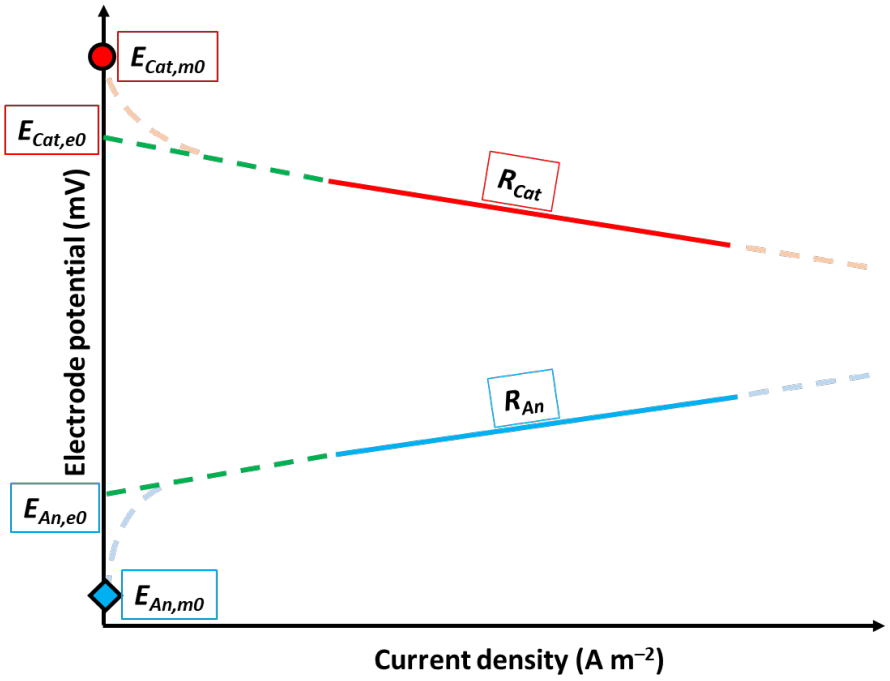

Schematic S1: Schematic representation of the parameters used for the EPS analysis. $E_{Cat,m0}$ and $E_{An,m0}$ are the cathodic and anodic potential measured at open circuit condition.The green dashed lines represent the linearization that would be obtained from polarization tests, and the intercept of this line with the *y*-axis has been used to calculate the cathodic ($E_{Cat,e0}$) and anodic ($E_{An,e0}$) experimental potential at zero current. The thick solid lines show the linearized portion of the polarization data that are used to calculate the anode (R_{An}) and cathode (R_{Cat}) resistances.

Diffusion through a stagnant layer in EIS spectra. Finite length linear diffusion describe the situation in which the mass transport in the close proximity of the electrode occurs only through diffusion. This phenomenon is typical for chemical species diffusing into thin films and then reacting. It is also common for fuel cells, when the hydrogen is oxydized at the electrode and the protons diffuse through the membrane. Outside of the diffusion layer the solution is homogeneous and the concentration of the species stable.

When a potential stimulus (5 mV amplitude in our case) is applied, the concentration of the species involved in the electrochemical reaction oscillates in function of their distance from the electrode and the frequency of the stimulus. At high frequencies, the concentration perturbation does not extend to the limit of the diffusion layer because the time for a molecule to diffuse across the thin layer is much longer than the period of the AC stimulus applied. At low frequencies, the perturbation of the concentration due to the stimulus extends to the limit of the diffusion layer and an abrupt change in the concentration of the diffusing species is observed at the limit of the stagnant film. Thus, at high frequencies, the oscillating concentration resembles that obtained for a stagnant medium of infinite dimension, while the behavior at low frequencies is influenced by the finite extent of the diffusion layer.

In the Nyquist plot, at high frequencies, the propagation of the disturbance away from the electrode surface lags behind the perturbation at the surface and a straight line will be obtained in the complex plane plot. At low frequencies, the concentration far from the surface responds with almost no phase lag. This will results, for frequencies tending toward zero, in a decrease in the imaginary part of the impedance and the formation of a semicircle. Thus, complex plane plots obtained in this conditions showed a straight line at 45° at high frequencies representative of a semi-infinite diffusional behavior followed by a semicircle intercepting the impedance on the real axis at low frequencies because in this conditions a dc current can flow.[1–3]

Analyzing the EIS spectra is possible to obtain informations on the thickness of the diffusion layer if the characteristic time (or frequency) of diffusion (t_{diff}) and the diffusivity of the chemical species is known. Using specific software for the analysis of the spectra allows to obtain t_{diff} directly from the fitting. However, the characteristic frequency of diffusion can be obtained from the intersection point between the convective diffusion impedance (the semicircle) and the straight line (due to semi-infinite diffusion) of pure diffusion impedance.[4] The characteristic frequency of diffusion in the example of Figure S1, can be approximated to be that of the yellow triangle point, correspondent to 84 mHz. The characteristic time of diffusion will then be $^{1}/_{84\ mHz} = 12\ s$.

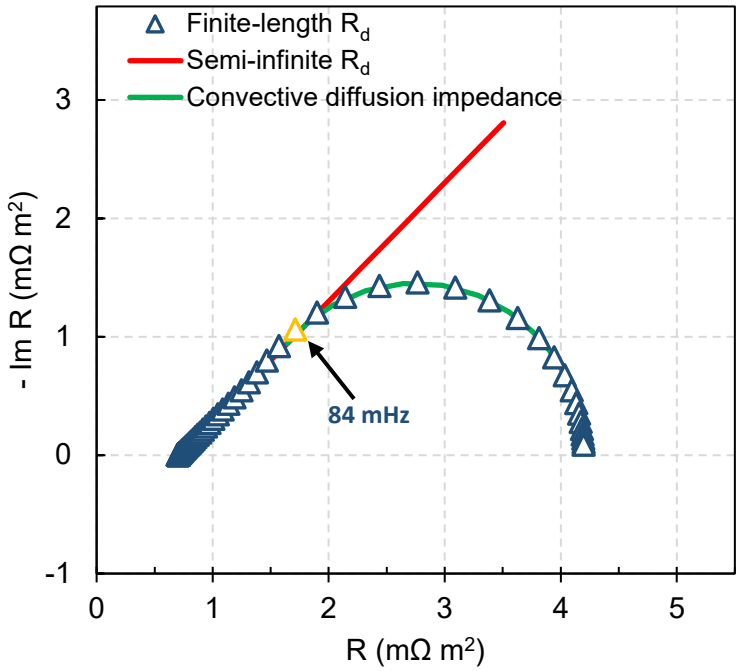

Figure S1: Nyquist plot of a typical finite-length diffusion impedance compared with semi-infinite diffusion impedance and the effect of a finite length diffusion layer thickness. The point where the imaginary impedance starts to decrease due to the finite length diffusion layer thickness is represented by the yellow triangle. The frequency of that point can be approximated to be the characteristic frequency of diffusion.

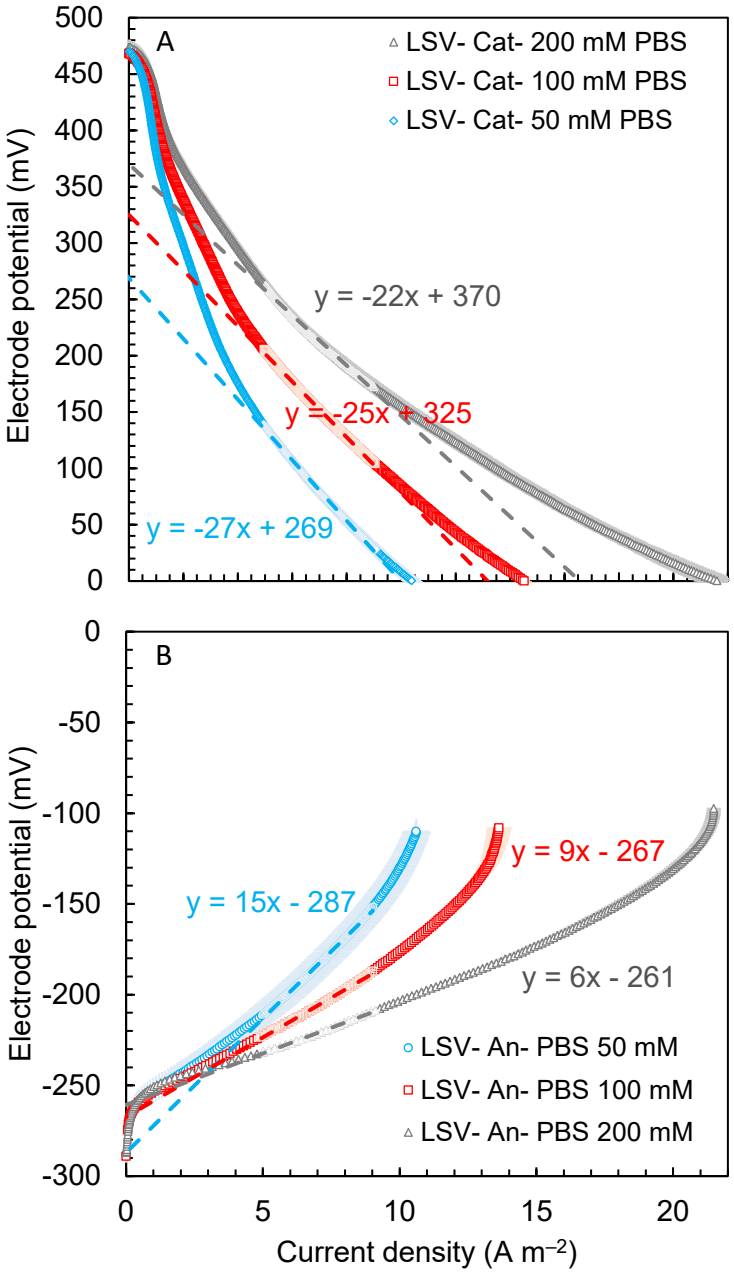

Figure S2: (A) Cathodic and (B) anodic linear sweep voltammetries in PBS at different concentrations (50 mM, 100 mM and 200 mM) not corrected for the solution resistance. The dashed lines represent the linearization of the data in the 5-9 A m^{-2} region.

EIS analysis of the cathode performance. EIS data to be valid needs to fulfill three conditions:[2,5]

1. Linearity: the perturbation of the potential applied through the AC must be small enough so that the response of the cell can be assumed to be linear (usually < 20 mVs);[6]
2. Causality: the response of the system should be directly correlated to the perturbation of the potential;
3. Stability: the overall state of the system must not change significantly during the acquisition of the data.

In our experiments the correspondence between the polarization resistance (R_p) and the charge transfer resistance (R_{CT}) (Figure 2B) fulfill the causality condition. The good agreement between the current obtained during the LSV (scan rate: 0.1 mV s^{-1}) and that achieved under steady conditions at the correspondent set potential in EIS analysis satisfy the stability condition.

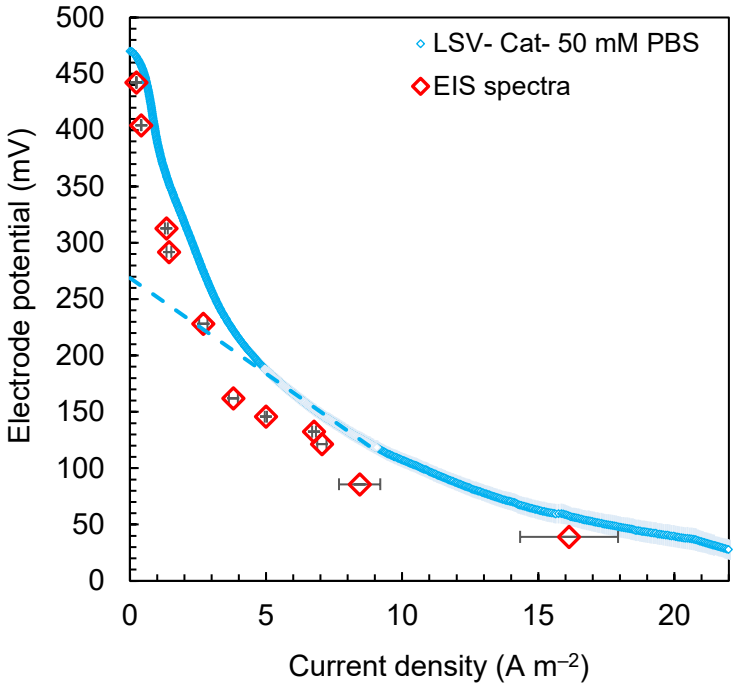

Figure S3. Comparison between the current density obtained at the correspondent cathode potentials in 50 mM PBS obtained from LSVs with a scan rate of 0.1 mV s^{-1} and in EIS experiments at a fixed electrode potential.

Cathode equivalent circuit. Two depressed semicircles were obtained in the Nyquist plot of the cathodes at each applied potential. Each semicircle was due to a different process. The spectra were fitted to the circuit in Figure S4 were R_Ω represents the solution resistance, Q_1/R_1 the ohmic related process and Q_{DL}/R_{CT} the kinetic process related to the ORR. R_Ω is the first intercept on the x axis at high frequencies, Q_1/R_1 is the first small semicircle and Q_{DL}/R_{CT} is the second, large, semicircle. A constant phase element (CPE, correspondent to *Q* in the circuit) was used for fitting the spectra instead of a pure capacitance. This is due to the fact that in our system the large porosity of the cathode resulted in an uneven distribution of the potential, resulting in a dispersion of the time constants.[7–9] This phenomenon is very common for highly porous materials, such our carbonaceous cathodes, and has been extensively explained in the literature.[1,2,9]

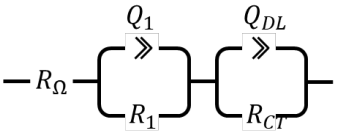

Impedance

$$Z = R_\Omega + \frac{R_1}{R_1 Q_1 (j\,2\,\pi\,f)^{\alpha_1} + 1} + \frac{R_{CT}}{R_{CT} Q_{DL} (j\,2\,\pi\,f)^{\alpha_{DL}} + 1}$$

Figure S4. Equivalent circuit used to fit the impedance diagrams of the cathodes recorded at different overpotentials.

EIS analysis of cathode in 50 mM PBS at low current overpotentials. At very low overpotentials and current densities, near the OCP, when activation losses predominate, the EIS spectra obtained at low frequencies (0.1 mHz) showed a third depressed semicircle following the kinetic one (Figure S5). The third semicircle was a kinetically-controlled process, likely due to a different cathodic reaction than that observed at current densities of 5-9 A m^{-2}. This third process likely arises from a different ORR that is favored only at a pH close to 7, which can be maintained by the buffer due to the low current density. The number of electrons transferred on AC cathodes usually ranges from 2.1-3.6,[10–12] due to the different ORR pathways that can occur on carbonaceous cathodes (Eq. 2, 3, 4, 5). For example, a direct 4 electron transfer to form water is favored at neutral pHs, while a 2 e^- transfer to hydrogen peroxide occurs at more alkaline pHs in PGM-free cathodes.[13] Thus, at a low current density and a pH close to 7 the ORR pathway to water occurs, but at higher current densities the pH would become more alkaline, favoring a different pathway. The presence of multiple ORR pathways could also explain the two slopes obtained from the Tafel plots (Figure S5). For example, with 200 mM PBS the first slope was 188 mV/dec, 28% lower than the 262 mV/dec obtained in 50 mM PBS, likely due to the higher effectiveness of the 200 mM PBS in maintaining a pH close to 7. Unfortunately, the two reactions evolved in a very close range of electrode potential, making it difficult to identify each of them with a rotating disk electrode analysis.

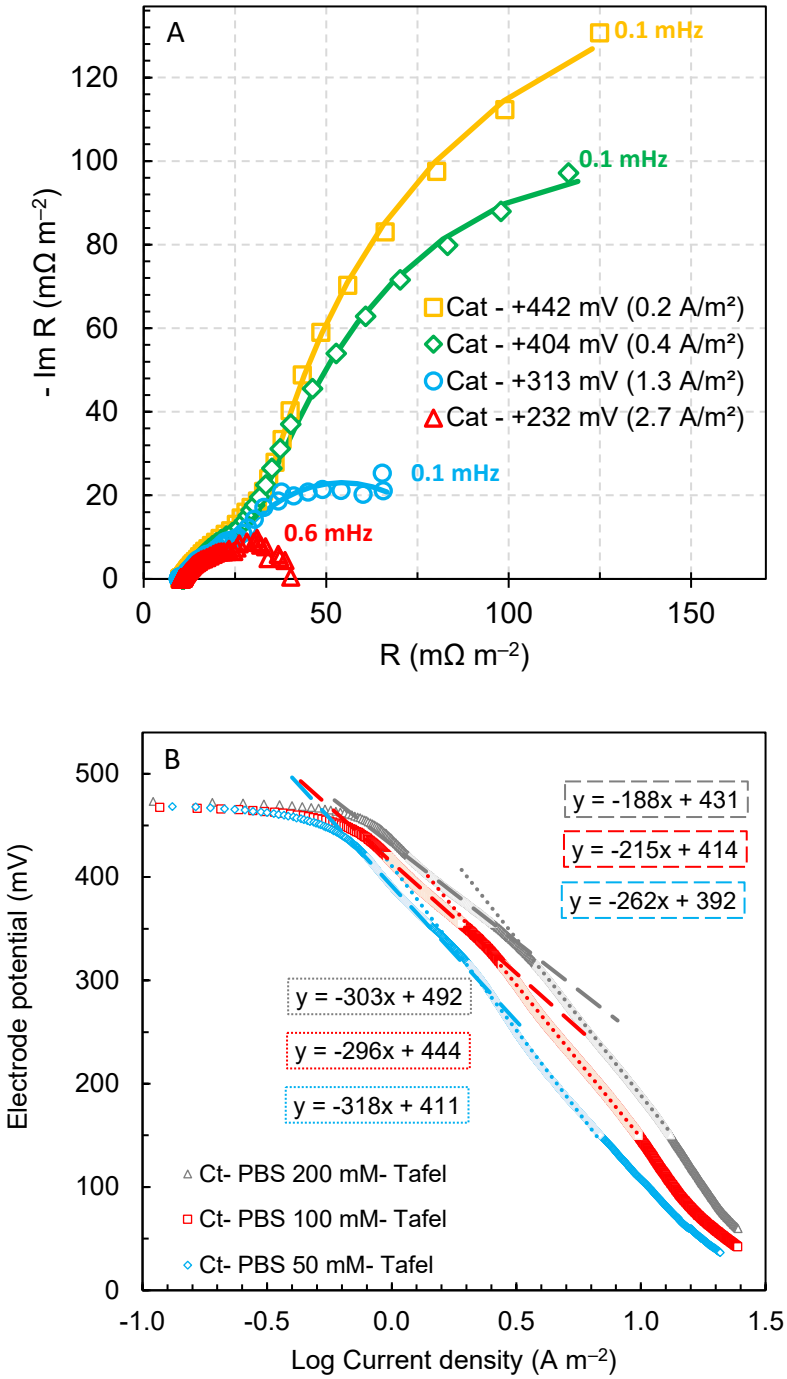

Figure S5. (A) Cathode EIS spectra in 50 mM PBS at current densities < 3 A m^{-2}. Solid lines represent the fitting to the data. The characteristic frequencies given in the plot for each spectrum correspond to the maximum in the imaginary impedance. (B) Tafel plot of cathode polarization in PBS 50 mM, 100 mM, and 200 mM. Conditions as in Figure 1A. The data were fit with a linear equation in the upper left (dashed line) over a 355-420 mV potential range, and the lower right (dotted line) over a 315-150 mV potential range.

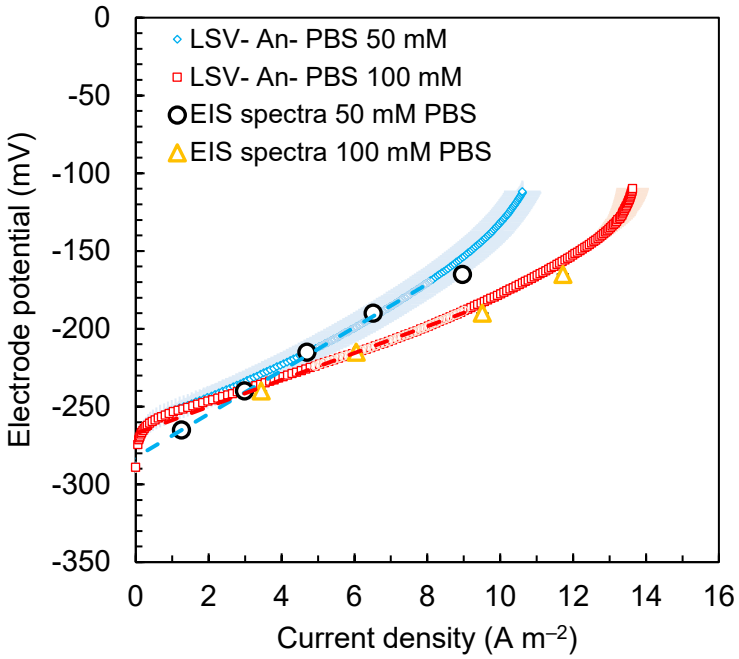

Figure S6. Comparison between the current density obtained at the correspondent anode potentials in 50 mM and 100 mM PBS obtained from LSVs with a scan rate of 0.1 mV s^{-1} and in EIS experiments at a fixed electrode potential.

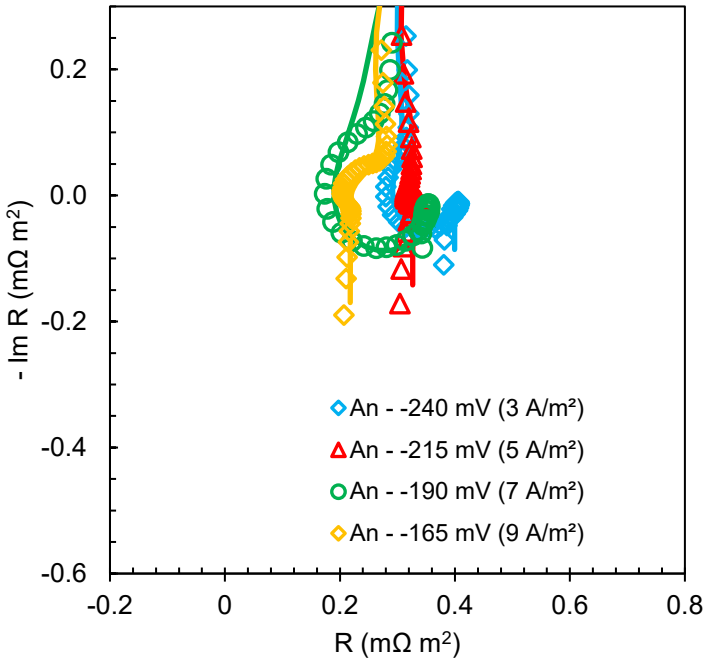

Figure S7. High frequencies part of the anode EIS spectra in 50 mM PBS. Solid lines represent the fitting to the data.

Anode equivalent circuit. The presence of several processes in the spectra complicated the definition of an equivalent circuit in respect to that used for the cathode (Figure S8). For example, the "loop" obtained close to the real impedance origin at high frequencies (Figure S7) could be fitted with inductive elements (L_2/R_2). These elements have been reported to be due to the large capacitance of the coaxial cables used in the electrochemical setup or to artifacts from the RE which are not an integral part of the MFC.[14–16] A small ohmic semicircle (Q_4/R_4), not visible in Figure 2, likely due to the small porosity of the graphite fibers, was obtained at each electrode potential but was independent by the applied potential and consequently, not involved in the electrochemical reaction. Previous studies have also identified this process and the correspondent capacitance with the electrochemically active biofilm.[7,17]

The circuits used to fit the spectra comprised inductive elements at high and low frequiencies. Induction at high frequencies is usually due to the wire connections and the measurement setup, but inductive behavior at low frequencies have struggled fuel cell researchers for many years.[18,19] Inductance is defined as the property of an electric circuit to develop an electromotive force due t a change in the current passing through the system itself. Inductance at low frequency have been identified with a change in the resistance of the electrochemical process over time.[18] Depending on the relative time of the change in the resistance in respect to the time constant of the electrochemical process a low frequency inductance could appear in the complex plane plots. These phenomena have been identified with side reactions with intermediate species,[14] catalyst poisoning,[14] wettability of the ion exchange membrane[18,19] but also with experimental artifacts.[15] As the anodic electron transfer in bioelectrochemical system involves several multi-step reactions,[20] it is likely that in our system, the induction is likely due to a two-step reaction, with the first reaction having a larger time constant than the consecutive ones.[18]

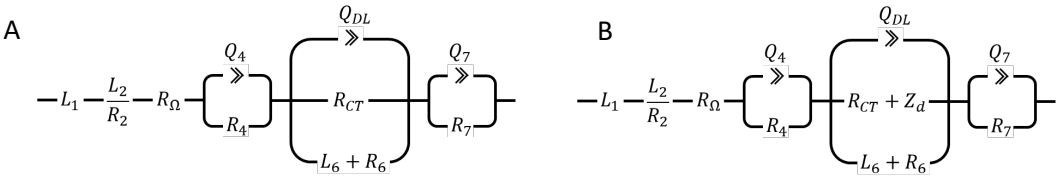

Figure S8. Equivalent circuit used to fit the impedance diagrams of the anodes (A) without and (B) with diffusion resistance recorded at different overpotentials.

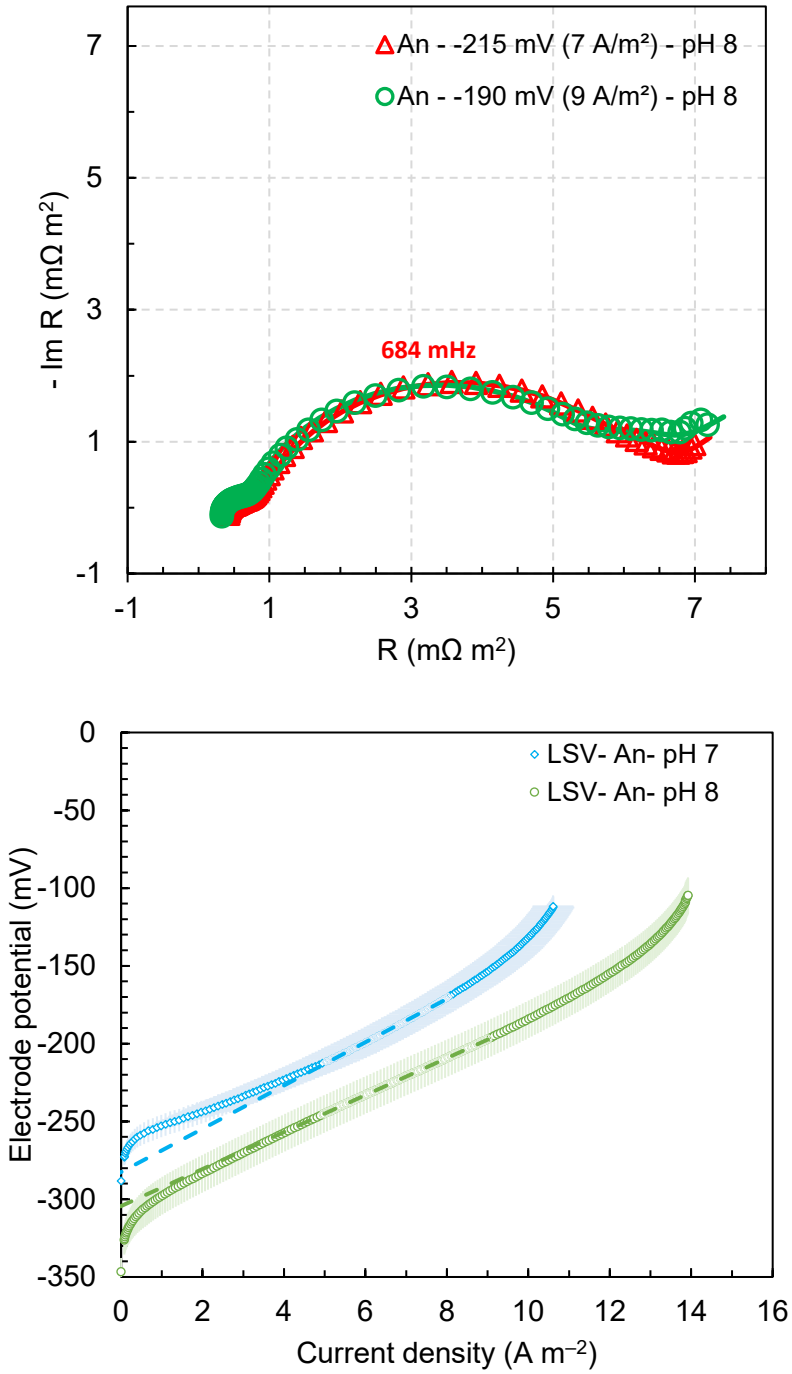

Figure S9. (A) Anode EIS spectra of the brushes in 50 mM PBS at pH 8. Solid lines represent the fitting to the data. The characteristic frequencies given in the plot for each spectrum correspond to the maximum in the imaginary impedance. (B) Anodic linear sweep voltammetries in 50 mM PBS at pH 7 or pH 8. The dashed lines represent the linearization of the data in the 5-9 A m^{-2} region.

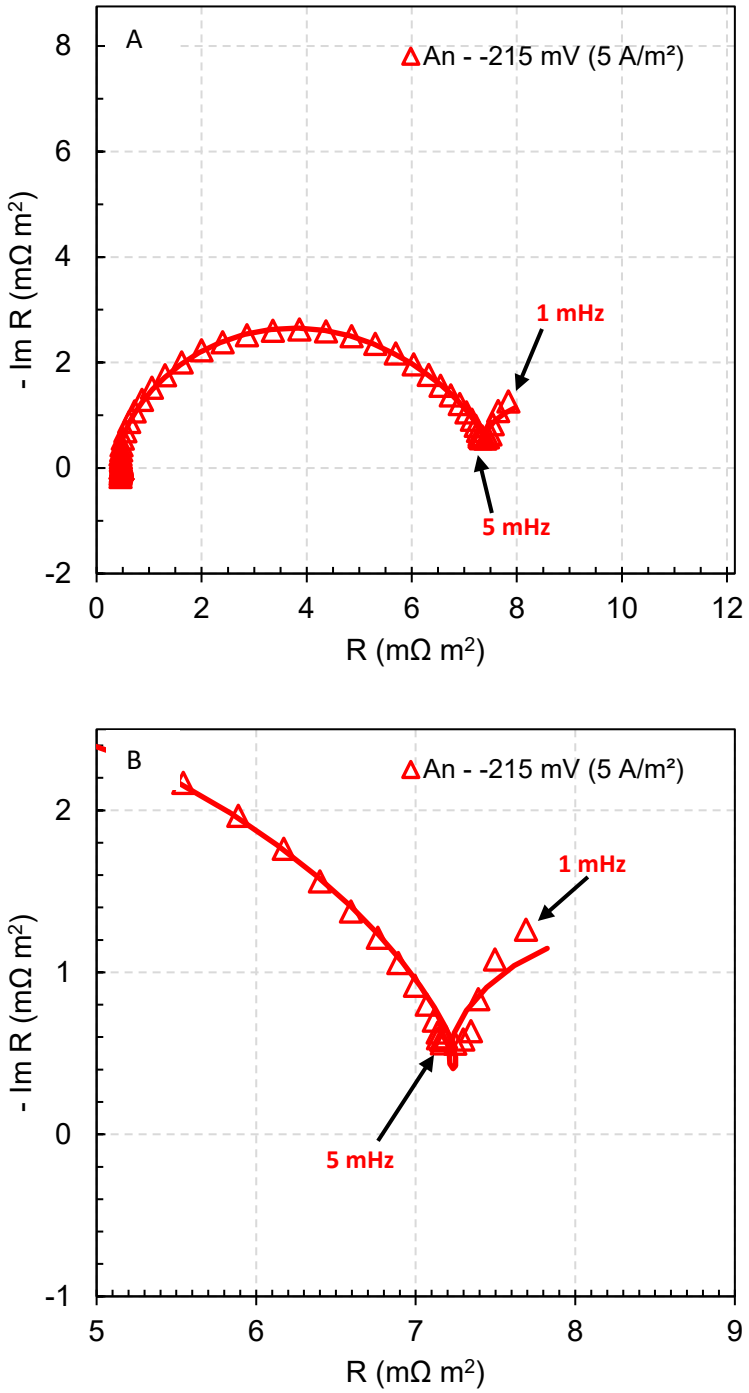

Figure S10. (A) Anode EIS spectra in 50 mM PBS scanned up to 1 mHz. Solid lines represent the fitting to the data. (B) Enlargement of the EIS spectra at low frequencies. The large semicircle is followed by a consecutive process only visible if the spectra is scanned at frequencies <5 mHz.

EIS response of brush anodes in PBS in 100 mM PBS. To investigate if a more concentrated buffer solution could reduce the impact of the diffusion resistance, the EIS spectra of the brush anodes were obtained in 100 mM PBS at the same overpotentials of that in 50 mM PBS (Figure S11). Diffusion resistance (R_d) was still observed in 100 mM, although appearing at more positive potentials and larger current densities (Figure S11, Figure S6). At electrode potentials more positive than –190 mV, R_d appeared in the Nyquist plots (Figure S11A). The diffusion resistance increased from 0.6 ± 0.1 mΩ m^2 at –190 mV (9.51 ± 0.01 A m^{-2}) to 1.7 ± 0.3 mΩ m^2 at –165 mV (11.72 ± 0.06 A m^{-2}). In 100 mM PBS, the diffusion of H^+ was still limiting the electrode performance. The charge transfer resistance in 100 mM PBS decreased from 6.5 ± 0.1 mΩ m^2 to 4.8 ± 0.8 mΩ m^2 by increasing the anode potential from –240 mV (3.4 ± 0.1 A m^{-2}) to –190 mV (9.51 ± 0.01 A m^{-2}) and then increased back to 5.57 ± 0.04 mΩ m^2 at –165 mV (11.72 ± 0.06 A m^{-2}), likely due to the adverse effect of acidification of the biofilm on the bacterial kinetic (Figure S11B).

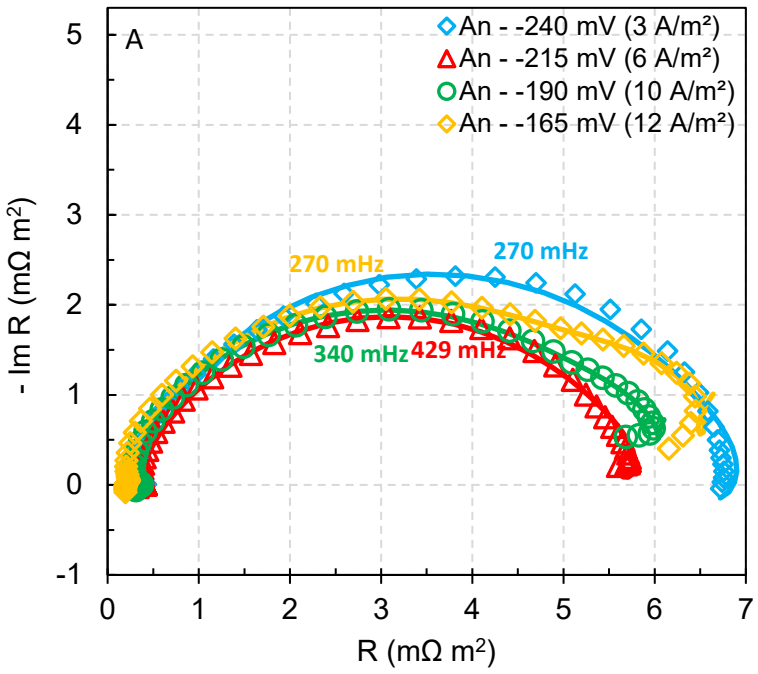

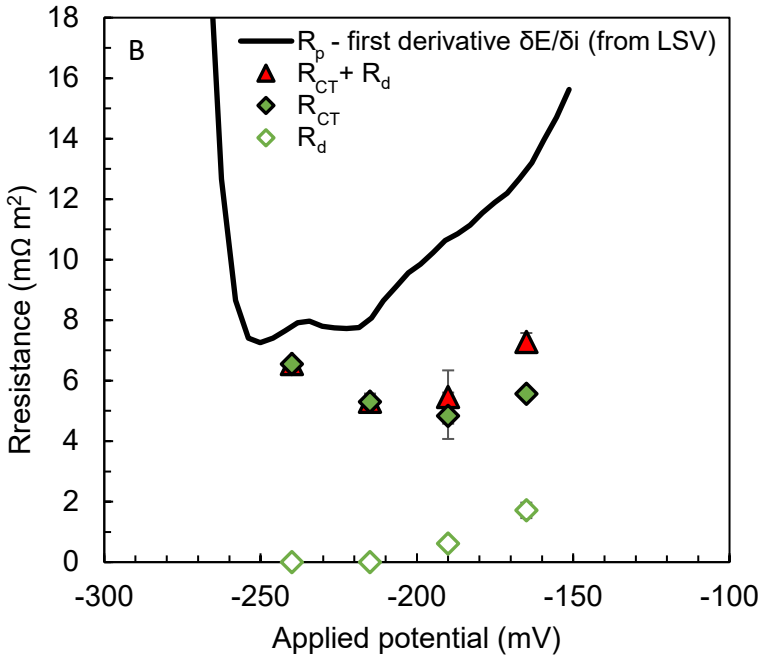

Figure S11. (A) Anode EIS spectra in 100 mM PBS. Solid lines represent the fitting to the data. The characteristic time frequencies correspondent to the maximum in the imaginary impedance are reported in the graph. (B) Correspondent anodic charge transfer (R_{CT}) and diffusion (R_d) resistance, obtained from the spectra, and polarization resistance (solid black line- R_p) calculated from the slope of the LSVs as $\delta E/\delta i$. The overpotential can be calculated from OCP = –289 ± 4 mV.

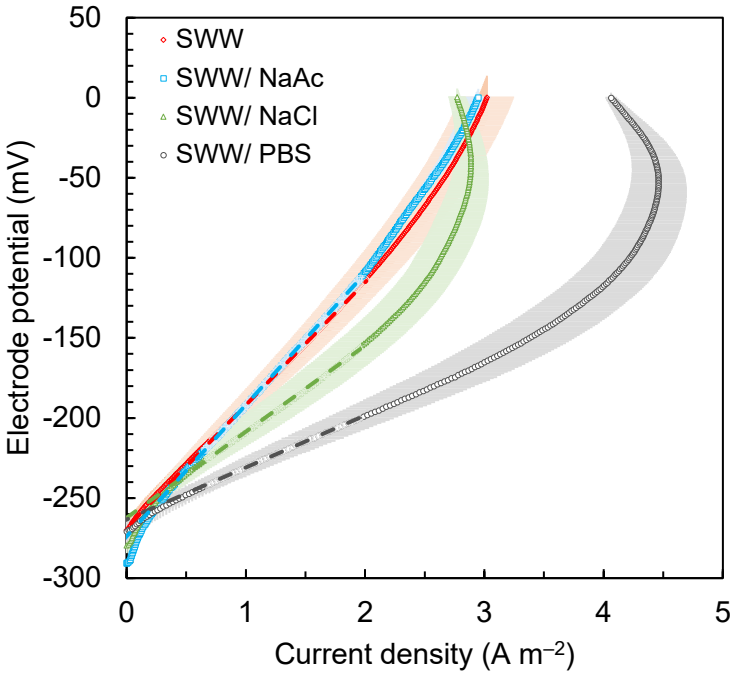

Figure S12. Anodic linear sweep voltammetries in synthetic wastewater and in synthetic wastewater amended with sodium acetate (SWW/NaAc), sodium chloride (SWW/NaCl) and phosphate buffer (SWW/PB) not corrected for the solution resistance. The dashed lines represent the linearization of the data in the 0.7-2.0 A m^{-2} region.

Impact of media used for acclimation on anode performance. Anode performance can also be impacted by the acclimation "history" and condition of the anode.[21] If buffer and substrate concentration were the only two important factors in anode performance, then adding 50 mM PBS and acetate to an anode would always produce the same outcome in LSVs. However, when both PBS and acetate were added to the MFCs with anodes that were acclimated to, and fed with, domestic wastewater for more than one year, the performance was much lower than anodes that were always fed with acetate in PBS for the same amount of time (Figure 3, Figure S13). The anode resistance decreased for SWW amended with both 50 mM PBS and additional sodium acetate (from 0.25 g L^{-1} to 0.50 g L^{-1} final concentration) by 25% (from $R_{An\ SWW\text{-}PB}$ = 28.1 ± 0.1 mΩ m^2 to $R_{An\ SWW\text{-}PB+NaAc}$ = 21.5 ± 0.2 mΩ m^2), and the limiting current density increased by 64% (from 4.4 ± 0.2 A m^{-2} to 7.2 ± 0.5 A m^{-2}) (Figure 3). Even with additional acetate in the medium the anode performance was still much less than that obtained using brush anodes fed only PBS and acetate medium for >1 year (Figure 3, Figure S13A). In addition, decreasing the concentration of acetate in PBS for these PBS-acetate acclimated anodes to 0.50 g L^{-1} or 0.25 g L^{-1} did not change their electrode performance (Figure S14). As a result of these different outcomes for the WW acclimated versus PBS-acetate acclimated anodes, it was concluded that the biofilm conditions, which was observed to be thick and inhomogeneous in WW fed anodes (Figure S13), was a major factor in anode performance.

Improvements in anode performance by adding additional acetate and PBS were much lower than that obtained using anodes fed with acetate and PBS for >1 year. The main reason for this lack of impact was likely due to a large accumulation of exopolymeric material in the brush anode acclimated in wastewater, which could account for the doubling of the anode resistance compared to anode acclimated only in acetate and PBS ($R_{An\text{-}PBS\ 50mM}$ = 9.08 ± 0.08 mΩ m^2 versus $R_{An\text{-}SWW/PB+NaAc}$ = 21.5 ± 0.2 mΩ m^2). These SWW tests therefore indicated that the once dense polymeric biofilms have accumulated on anodes acclimated to low strength wastewaters, performance will not improve with more optimal

conditions likely due to the polymeric materials hindering diffusion of molecules to and from the anode biofilm.

Figure S13. Brush anode photos. The pictures were taken on the anode facing the cathode, in MFCs fed with (A) PBS for > 1 year and (B) wastewater for > 2 years. The cells were used for other experiments during this time.

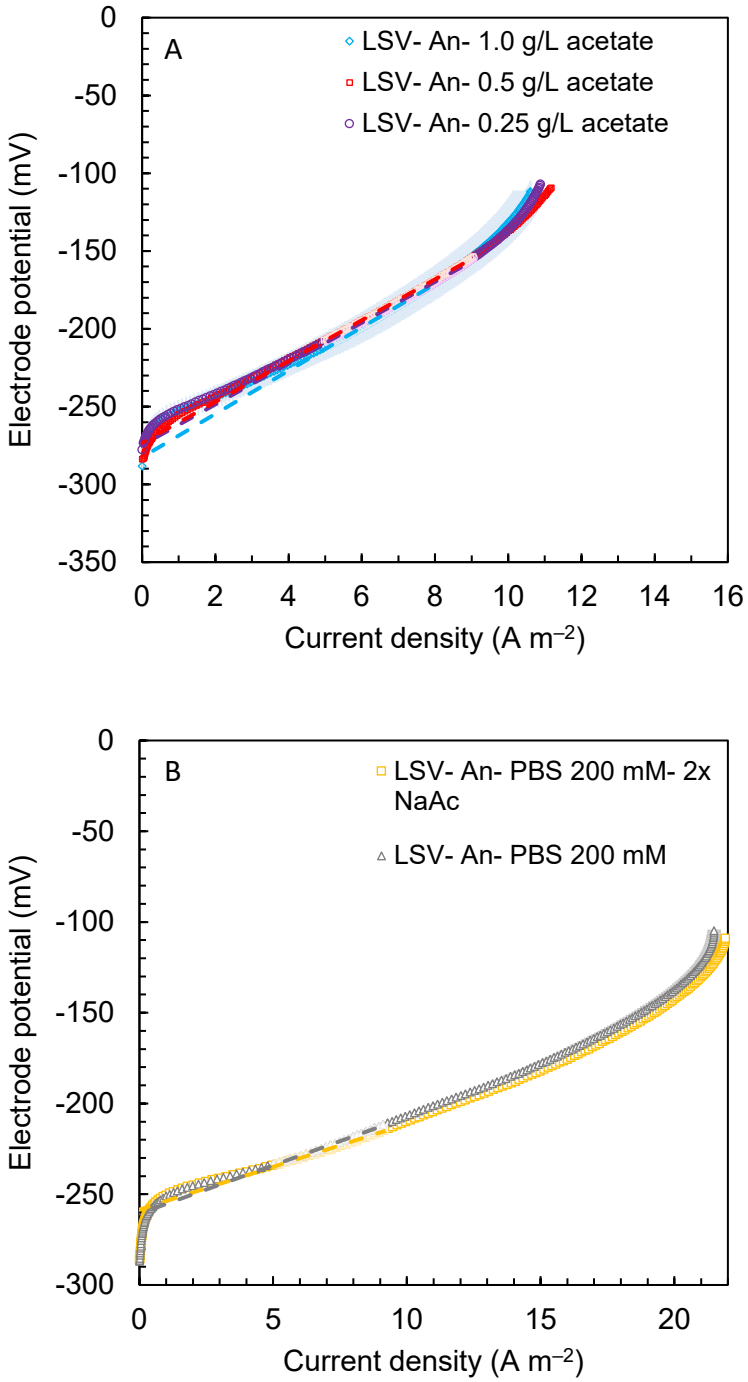

Figure S14. (A) Anodic linear sweep voltammetries in 50 mM PBS at pH 7 with 1.00, 0.50 or 0.25 g L^{-1} sodium acetate. The dashed lines represent the linearization of the data in the 5-9 A m^{-2} region. (B) Anodic linear sweep voltammetries in 200 mM PBS at pH 7 with 1 or 2 g L^{-1} sodium acetate. The dashed lines represent the linearization of the data in the 5-9 A m^{-2} region.

Table S1. Characteristic of the primary effluent wastewater collected at the Pennsylvania State University Wastewater Treatment Plant.

	PRIMARY SETTLING EFFLUENT								
	11/16/2012 6:45:00 AM	11/17/2012 7:00:00 AM	11/18/2012 7:00:00 AM	11/19/2012 7:00:00 AM	11/20/2012 6:50:00 AM	11/21/2012 6:40:00 AM	11/22/2012 6:50:00 AM		
Flow Rate (mgd)	2.13	2.02	1.78	1.17	1.33	1.37	1.22	Average 7 days	S.D.
Day of the week	Friday	Saturday	Sunday	Monday	Tuesday	Wednesday	Thursday		
Calcium (mg/L)	69	10	66	71	73	66	62	60	21
Copper (mg/L)	0.09	0.14	0.08	0.11	0.18	0.10	0.12	0.12	0.03
Mercury (mg/L)	ND	ND	ND	ND	ND	ND	ND	ND	ND
Potassium (mg/L)	13	12	15	10	11	10	8	11	2
Magnesium (mg/L)	31	29	28	29	31	28	27	29	1
Sodium (mg/L)	190	196	169	199	223	147	222	192	25
Zinc (mg/L)	0.07	0.08	0.07	0.08	0.09	0.09	0.06	0.08	0.01
Biochemical Oxygen Demand (mg/L)	167	189	169	108	182	95	174	155	35
Biochemical Oxygen Demand (Soluble) (mg/L)	100	83.1	89.8	42.7	67.7	27.2	52.5	66	25
Chemical Oxygen Demand (mg/L)	321	287	307	246	356	228	258	286	42
Chemical Oxygen Demand (Soluble) (mg/L)	127	138	149	87.5	140	67	78.4	112	31
Total Alkalinity (mg/L)	386	380	390	350	320	280	310	345	40
Chloride (mg/L)	318	338	286	327	399	241	349	323	46
Sulfate as SO4 (mg/L)	37	35	35.2	37.9	33.3	32.5	33.7	35	2
Phosphorus (mg/L)	5.6	6.0	6.2	4.6	5.2	6.3	3.8	5.4	0.9
Phosphorus (Dissolved) (mg/L)	3.7	4.0	4.0	2.6	3.0	4.9	1.1	3.3	1.1
Orthophosphate as P (mg/L)	3.1	3.6	4.1	2.5	2.7	4.0	2.2	3.2	0.7
Nitrate as N (mg/L)	ND	ND	ND	ND	ND	ND	ND	ND	ND
Nitrite as N (mg/L)	ND	ND	ND	ND	ND	ND	ND	ND	ND
Total Kjeldahl Nitrogen (mg/L)	51.7	51.11	57.01	39.34	29.94	30.69	17.06	40	13
Ammonia as N (mg/L)	38.9	35.35	45.16	28.89	27.7	23.79	18.11	31	9
Total Kjeldahl Nitrogen (Soluble) (mg/L)	41.46	38.28	48.96	25.49	21.91	22.16	20.2	31	11
Total Dissolved Solids (mg/L)	890	899	780	898	1000	770	927	881	75
Total Suspended Solids (mg/L)	64	60	60	73	118	49	57	69	21
Volatile Suspended Solids (mg/L)	64	52	56	69	106	46	52	64	19
pH	7.9	7.3	7.6	7.6	7.4	7.7	7.4	7.6	0.2

References

[1] M.E. Orazem, B. Tribollet, Electrochemical Impedance Spectroscopy, 2008th ed., John Wiley & Sons, Inc.,Publication, Hoboken, New Jersey, 2008.

[2] A. Lasia, Electrochemical impedance spectroscopy and its applications, Springer, New York Heidelberg Dordrecht London, 2014. doi:10.1007/978-1-4614-8933-7.

[3] J. Bisquert, G. Garcia-Belmonte, F. Fabregat-Santiago, P.R. Bueno, Theoretical models for AC impedance of finite diffusion layers exhibiting low frequency dispersion, J. Electroanal. Chem. 475 (1999) 152–163. doi:10.1016/S0022-0728(99)00346-0.

[4] S. Sanchez, S. Cassaignon, J. Vedel, H. Gomez Meier, Copper diffusion in solid copper sulfide electrode, Electrochim. Acta. 41 (1996) 1331–1339.

[5] M. Urquidi-Macdonald, S. Real, D.D. Macdonald, Applications of Kramer-Kronig transforms in the analysis of electrochemical impedance data, Electrochim. Acta. 35 (1990) 1559–1566.

[6] F. Fasmin, R. Srinivasan, Review—Nonlinear electrochemical impedance spectroscopy, J. Electrochem. Soc. 164 (2017) H443–H455. doi:10.1149/2.0391707jes.

[7] X. Dominguez-Benetton, S. Sevda, K. Vanbroekhoven, D. Pant, The accurate use of impedance analysis for the study of microbial electrochemical systems, Chem. Soc. Rev. 41 (2012) 7228–7246. doi:10.1039/c2cs35026b.

[8] B. Hirschorn, M.E. Orazem, B. Tribollet, V. Vivier, I. Frateur, M. Musiani, Determination of effective capacitance and film thickness from constant-phase-element parameters, Electrochim. Acta. 55 (2010) 6218–6227. doi:10.1016/j.electacta.2009.10.065.

[9] G.J. Brug, A.L.G. van den Eeden, M. Sluyters-Rehbach, J.H. Sluyters, The analysis of electrode impedances complicated by the presence of a constant phase element, J. Electroanal. Chem. 176 (1984) 275–295. doi:10.1016/S0022-0728(84)80324-1.

[10] W. Yang, B.E. Logan, Immobilization of a metal-nitrogen-carbon catalyst on activated carbon with enhanced cathode performance in microbial fuel cells, ChemSusChem. 9 (2016) 2226–2232. doi:10.1002/cssc.201600573.

[11] V.J. Watson, C. Nieto Delgado, B.E. Logan, Influence of chemical and physical properties of activated carbon powders on oxygen reduction and microbial fuel cell performance, Environ. Sci. Technol. 47 (2013) 6704–6710. doi:10.1021/es401722j.

[12] C. Santoro, M. Kodali, S. Kabir, F. Soavi, A. Serov, P. Atanassov, Three-dimensional graphene nanosheets as cathode catalysts in standard and supercapacitive microbial fuel cell, J. Power Sources. 356 (2017) 371–380. doi:10.1016/j.jpowsour.2017.03.135.

[13] S. Rojas-Carbonell, K. Artyushkova, A. Serov, C. Santoro, I. Matanovic, P. Atanassov, Effect of pH on the activity of platinum group metal-free catalysts in oxygen reduction reaction, ACS Catal. 8 (2018) 3041–3053. doi:10.1021/acscatal.7b03991.

[14] I. Pivac, F. Barbir, Inductive phenomena at low frequencies in impedance spectra of proton exchange membrane fuel cells – A review, J. Power Sources. 326 (2016) 112–119. doi:10.1016/j.jpowsour.2016.06.119.

[15] H. Brandstätter, I. Hanzu, M. Wilkening, Myth and reality about the origin of inductive loops in impedance spectra of lithium-ion electrodes - A critical experimental approach, Electrochim. Acta. 207 (2016) 218–223. doi:10.1016/j.electacta.2016.03.126.

[16] B.W. Veal, P.M. Baldo, A.P. Paulikas, J.A. Eastman, Understanding artifacts in impedance spectroscopy, J. Electrochem. Soc. 162 (2015) H47–H57. doi:10.1149/2.0791501jes.

[17] A. ter Heijne, D. Liu, M. Sulonen, T. Sleutels, F. Fabregat-Santiago, Quantification of bio-anode capacitance in bioelectrochemical systems using Electrochemical Impedance Spectroscopy, J. Power Sources. 400 (2018) 533–538. doi:10.1016/j.jpowsour.2018.08.003.

[18] D. Klotz, Negative capacitance or inductive loop? – A general assessment of a common low frequency impedance feature, Electrochem. Commun. 98 (2019) 58–62.

doi:10.1016/j.elecom.2018.11.017.
[19] S.K. Roy, M.E. Orazem, B. Tribollet, Interpretation of low-frequency inductive loops in PEM fuel cells, J. Electrochem. Soc. 154 (2007) B1378. doi:10.1149/1.2789377.
[20] S.M. Strycharz, A.P. Malanoski, R.M. Snider, H. Yi, D.R. Lovley, L.M. Tender, Application of cyclic voltammetry to investigate enhanced catalytic current generation by biofilm-modified anodes of Geobacter sulfurreducens strain DL1 vs. variant strain KN400, Energy Environ. Sci. 4 (2011) 896–913. doi:10.1039/c0ee00260g.
[21] D. Sun, J. Chen, H. Huang, W. Liu, Y. Ye, S. Cheng, The effect of biofilm thickness on electrochemical activity of Geobacter sulfurreducens, Int. J. Hydrogen Energy. 41 (2016) 16523–16528. doi:10.1016/j.ijhydene.2016.04.163.